Indian Journal of Pure & Applied Physics
Vol. 59, July 2021, pp. 483-489

# A Compact High Sensitive D Shape Surface Plasmon Sensor

S Nivedha[a] & K Senthilnathan[b*]

[a]School of Electronics Engineering, Vellore Institute of Technology, Vellore 632 014, India

[b]Department of Physics, School of Advanced Sciences,Vellore Institute of Technology, Vellore, 632 014, India

*Received 5 May 2021; accepted 8 June 2021*

In this paper, we numerically design a refractive index-based surface plasmon fiber sensor by exploiting the optical characteristics of a commercially available side polished D-shaped photonic crystal fiber (PCF) using finite element method. The proposed sensor could work in the infrared regime for a wide range of analytes with refractive indices ranging from 1.33 to 1.36. The proposed sensor exhibits a maximum sensitivity of 31,800 nm/RIU with a resolution of $3.14\times10^{-6}$ RIU when the refractive index is varied from 1.355 to 1.36. Further, considering the practical implementation, we carry out the fabrication tolerance of ± 5% of the proposed sensor by varying the optimized structural parameters. Based on the numerical results, we find that the proposed sensor is highly robust against the variations in the structural parameters. As the proposed fiber sensor has a strong surface plasmon resonance between the core mode and the surface plasmon mode, it is highly sensitive even for a minimum change in the refractive index of the analyte which is an attribute of high preference in biosensors.

**Keywords:** D-shaped fiber sensor, Photonic crystal fiber, Refractive index, Surface plasmon resonance.

## 1 Introduction

In past few decades, surface plasmon resonance (SPR) technique has been widely used in physical, chemical and biological fields[1,2] and also in food safety[3,4] due to its simple design, high sensitivity and label free detection of analyte samples. Owing to the compact probe design, robustness and capability of detecting multiple samples in real time, SPR based sensors extend applications in medical diagnosis, chemical interactions and analysis in the micro molecular level[5]. SPR is an optical phenomenon that occurs during the total internal reflection (TIR) when a plane polarized light is incident on the dielectric-metal interface at an angle greater than the critical angle. Even though the light is totally reflected, some of the incident light leaking through the dielectric-metal interface gives rise to evanescent waves. These evanescent waves decay exponentially in nature but excite the surface plasmons that reside on the top of metal surface. The excited surface plasmon waves oscillate between the metal and the surrounding dielectric medium. When the frequencies of the incident wave and that of the surface plasmon match, resonance occurs[6]. This resonance wavelength is extremely sensitive to the minimal change in refractive index of the surrounding dielectric medium. The first anomaly of surface plasmons was observed by R W Wood in 1902[7]. Nonetheless a clear understanding of the SPR phenomenon was established in 1968 by Otto using the prism-based configuration[8]. Then, in the same year, Kretschmann and Raether proposed the well-known Kretschmann-Reather configuration that has been in vogue for SPR based sensing platform[9].Later, optical fibers have replaced prism configuration for realizing SPR sensors [10,11]. In optical fiber SPR sensors, a small portion of cladding is removed and coated with a metal layer. Here, the evanescent wave decays exponentially in the cladding region and TIR occurs at the boundary of the core and the cladding regions. In recent times, a special fiber called photonic crystal fiber (PCF) has been successfully deployed in realizing SPR sensors owing to small size and design flexibility of PCF. PCFs are dielectrics constructed with microscopic air holes arranged in a periodic array that run throughout the fiber[12]. PCF sensors are preferred to conventional fiber sensors due to compactness, efficient sensing, tunable birefringence, easy fabrication and adjustable dispersion[13-16]. It is also possible to attain a wide sensing range by optimizing the structural parameters. Besides, the selection of plasmonic supported material also plays an important role in PCF-SPR sensors. Of the various metals, Gold (Au) is considered to be the best material because of its lower oxidation, lower

*Corresponding author (E-mail: senthee@gmail.com)

corrosion and superior optical reactions[17]. Further, Au also does exhibit a sharp and narrow resonance peak[18].

To date, numerous D shaped SPR sensors have been reported. Wang *et al.* designed a PCF with square lattice whose wavelength sensitivity was 12,450 nm/RIU[19]. In 2017, a D shaped PCF based SPR sensor was proposed with a sensitivity of 7700 nm/RIU and a resolution of1.30 × $10^{-5}$ RIU[20]. Hasan *et al.,* demonstrated a SPR biosensor-based on dual-polarized spiral PCF that exhibits a maximum sensitivity of 4600 and 4300 nm/RIU in x- and y polarized modes, respectively[21]. Tong *et al.* developed a three core PCF SPR sensor whose refractive index sensitivity was 3435 nm/RIU in the sensing range of 1.33–1.40 and a resolution of 2.91 ×$10^{-6}$RIU[22]. Zhou *et al.*. proposed a practical sensor based on SPR in a ring-shaped core PCF that displayed a maximum wavelength of 6900 nm/RIU in the analyte RI range from 1.33 to 1.41[23].Sakib *et al.* proposed a high-performance dual core D shape PCF SPR sensor with a supreme wavelength sensitivity of 8000 nm/RIU and resolution of 1.25 × $10^{-5}$ RIU[24]. Liao *et al.* developed a birefringent six-core PCF sensor. By using the full-vector finite element method, an average sensitivity of 8083 nm/RIU and resolution of 5.98×$10^{-6}$ RIU were reported[25]. Very recently, a D shaped PCF with V-groove analyte channel was demonstrated with a sensitivity of 31,600 nm/RIU and resolution of 3.16×$10^{-6}$RIU[26].

In this paper, we design a commercially available side polished D-shaped PCF with hexagonal lattice and explore the optical characteristics for realizing an SPR sensor. By side polishing the PCF, we successfully access the core region which enhances the interaction between core and surface plasmon region. In Section 2, we use the finite element method for designing a commercially available side polished D-shaped PCF with hexagonal lattice. We delineate the physical mechanism of the proposed sensor in Section 3. Then, we optimize the various structural parameters, namely, air-hole diameter, pitch and thickness of the gold layer in Section 4. Finally, we explore the robustness of the proposed sensor against the variations in various structural parameters in Section 5. Section 6 presents the crux of the research work.

## 2 Structure and theoretical modeling of the proposed sensor

The cross-section of side polished D shaped PCF is shown in Fig. 1. The air hole diameter of the first ring, d1, is 1.2 μm and that of second ring, d2, is 1.6 μm. The air holes are arranged in triangular lattice and the distance between two air holes, pitch (Λ), is kept as 2.2 μm. The proposed sensor is designed by removing the top two layers of air holes.

Silica forms the background material whose refractive index is calculated by Sellmeier's equation and the same is given by [27]

$$n(\lambda) = \sqrt{1 + \frac{B_1\lambda^2}{\lambda^2 - C_1} + \frac{B_2\lambda^2}{\lambda^2 - C_2} + \frac{B_3\lambda^2}{\lambda^2 - C_3}} \quad \ldots(1)$$

The Sellmeier constants for $B_1$, $B_2$, $B_3$, $C_1$, $C_2$ and $C_3$ fused silica are 0.69616300, 0.407942600, 0.897479400, 0.00467914826, 0.0135120631 & 97.9340025, respectively.

In this PCF, a thin layer of gold of thickness of 40 nm is deposited on the polished surface. The dielectric constant of gold layer is calculated using Drude model[28] and the same is given as,

$$\varepsilon(\lambda) = \varepsilon_\infty - \frac{\lambda^2\lambda_c}{\lambda_p^2(\lambda_c + i\lambda)}. \quad \ldots(2)$$

Here, $\lambda_p$ and $\lambda_c$ are the dispersion coefficients in micrometres. $\lambda_p$ is the plasma frequency for the corresponding wavelength of 0.56497 μm and $\lambda_c$ is the collision wavelength ($\lambda_c$ = 11.21076). Here the incident wavelength, λ, is measured in micrometres. The refractive index of analyte is varied from 1.33 to 1.36 in steps of 0.005. We employ finite element method to study mode propagation of the proposed sensor. The PCF is investigated using COMSOL multiphysics software. Here, the boundary conditions are applied by using perfectly matched layer which absorbs the radiated light energy emitted towards the surface of the fiber[29]. As the air hole diameters of the first, second and third rings are within the fabrication range, we envisage that the proposed D-shaped PCF can either be directly fabricated by half way stacking or by fabricating a regular PCF followed by

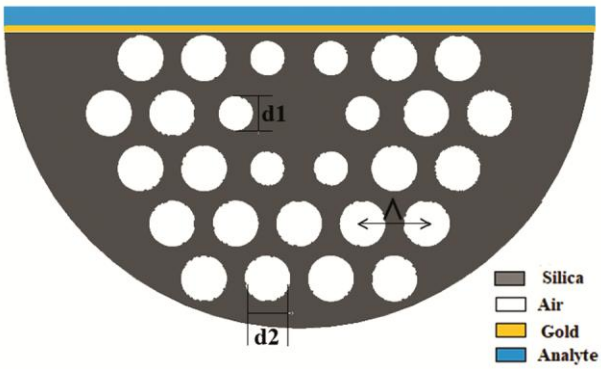


Fig. 1 — Cross-sectional view of the proposed D-shaped PCF sensor

mechanical side polishing[30,31]. Further, the desired gold layer can be deposited using a chemical deposition method[32].

## 3 Physical mechanism of the D-shaped PCF sensor

As a first step, we calculate the real and imaginary parts of effective refractive index (RI), $n_{eff}$, as a function of wavelength. Then, we compute the confinement loss using the imaginary part of $n_{eff}$. The confinement loss is calculated using the following expression[33],

$$\alpha_{loss} = 8.686 \times \frac{2\pi}{\lambda} \times Im(n_{eff}) \times 10^4 (dB/cm) \quad ...(3)$$

Here, $Im(n_{eff})$ represents the imaginary part of the effective RI of the fundamental mode which accounts for the loss and λ is the operating wavelength in μm. Fig. 2 depicts the loss spectrum and the dispersion relation of a core guided mode and plasmon mode when refractive index of analyte is 1.33 for a gold layer thickness of 40 nm. At this juncture, in SPR sensor, it is essential to establish the phase matching between the fundamental mode and surface plasmon mode.

In order to establish the same, we find the dispersion relation of fundamental mode and surface plasmon mode and the same is plotted in Fig. 2. The phase matching condition occurs at a resonance wavelength of 1677 nm, where maximum energy is transferred from fundamental mode to plasmon mode. Besides, we also compute the confinement loss to confirm that the energy transfer takes place from the fundamental mode to surface plasmon mode. From Fig. 2, it is very clear that the confinement loss of a fundamental mode turns maximum at the phase matching wavelength of 1677 nm. The maximum loss of the fundamental mode is mainly because of the energy transfer into the lossy plasmon mode. Thus, the coincidence of the peak of the loss spectrum and the intersection point between fundamental and surface plasmon modes clearly reveal the phase matching phenomenon.

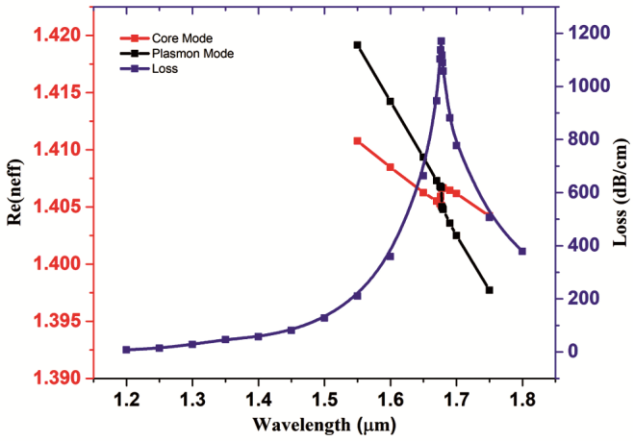


Fig. 2 — Loss curve and dispersion relation between the fundamental and the plasmon modes for the analyte RI, na = 1.33 and gold layer thickness t = 40 nm

It should be emphasized that the identification of a maximum loss of the fundamental mode at the phase matching point is treated as one of the main design criteria in plasmonic sensors.

## 4 Optimization of the proposed D-shaped PCF

Having discussed the physical mechanism of the proposed D-shaped PCF sensor in the previous section, in this section, we delineate the optimization of the structural parameters by varying geometrical parameters, namely, thickness of gold layer, radius of the first ring air holes and pitch of the air holes.

### 4.1 Variation of gold layer thickness

Now, we analyze the loss spectra for various gold layer thicknesses in order to identify the optimized one. Figure 3 shows the variations of gold layer thicknesses for three different analytes with refractive indices, 1.35, 1.355 and 1.36. It is seen from Fig. 3 that there is a resonant wavelength shift of 41 nm when the analyte is varied from 1.355 to 1.36 for a gold layer thickness of 45 nm. However, there is a maximum shift of 159 nm in the resonant wavelength for a gold layer thickness of 40 nm. Moreover, when the thickness of the gold layer is reduced to 35 nm, the peak shift reduces to 30 nm. In addition, there is a broadening in the loss curve which ultimately brings down the performance and accuracy of the sensor. Hence, the thickness of the gold layer has been optimised to be 40 nm in the proposed sensor and

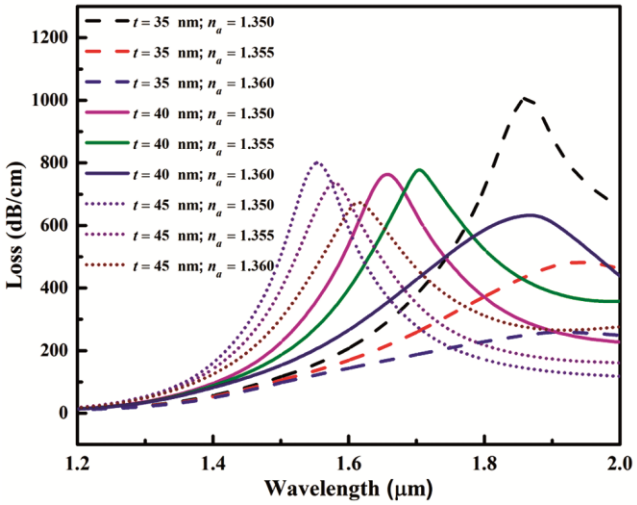


Fig. 3 — Loss spectra for three different gold thicknesses (35,40,45 nm) when the RI of analyte is varied from 1.35 to 1.36

the rationale behind the same follows from the above discussion.

#### 4.2 Variation of air-hole diameter

The variation of first ring air hole diameter, d1, for different analyte refractive indices of 1.33, 1.335 and 1.34 is depicted in Fig. 4. It is observed that, for d1 = 1.2 μm, there is a shift of 17 nm in the resonant wavelength when the RI of analyte is increased from 1.335 to 1.34 and this results in a sensitivity of 3400 nm/RIU. However, when the diameter of the air-hole is decreased to 1.0 μm, there is only a small variation of 14 nm shift in the resonant wavelength. Finally, for d1 = 1.4 μm, a shift of 13 nm is observed for the same variation of analyte's RI which is accompanied by a very low loss and broader loss spectra as depicted in Fig. 4. Based on the above discussion, the first ring air hole diameter is optimized to be 1.2 μm.

#### 4.3 Variation of pitch

Figure 5 depicts the variations of loss spectra for three different RIs (1.33, 1.335 and 1.34) when the pitch is varied from 2 to 2.4 μm. Here, with increase in pitch value, it is observed that the resonant wavelengths undergo red shift but there is no appreciable change in the peak loss. Further, for higher pitch values, the loss spectra get broadened. It is observed that for 2 μm pitch, when the refractive index of the analyte is varied from 1.33 to 1.335, there is a shift in peak wavelength of 10 nm and the peak wavelength is shifted by 11 nm for a pitch of 2.4 μm. On the other hand, for a pitch of 2.2 μm, when the RI is varied from 1.33 to 1.335, a peak wavelength shift of 14 nm is observed. Thus, a pitch of 2.2 μm is optimized.

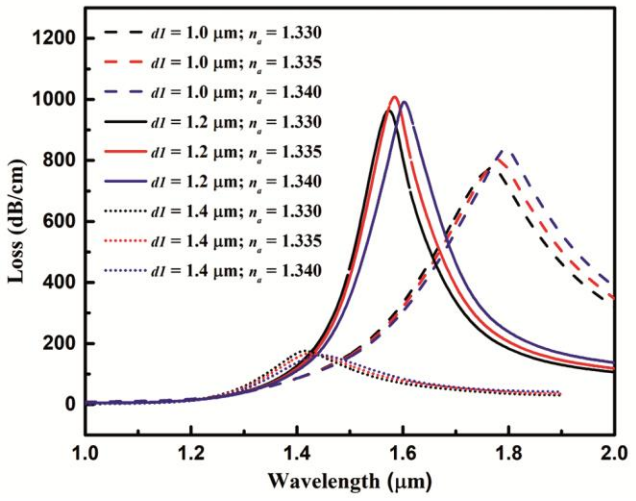


Fig. 4 — Loss spectra for three different air hole diameter d1 when the RI of analyte is varied from 1.35 to 1.36

The sensitivity is calculated by wavelength interrogation method by the expression[34]

$$S(\lambda) = \frac{\Delta\lambda_{peak}}{\Delta n_a} nm/RIU, \quad \ldots (4)$$

Where $\Delta\lambda_{peak}$ is the shift in peak wavelength in nm and $\Delta n_a$ is change in RI of analyte. Having analyzed the physical mechanism of the surface plasmon sensor for a single analyte (1.33) and optimization of various structural parameters, the next step is to examine the versatility of the proposed sensor when the refractive index of the analyte is varied slightly from the above-mentioned value.

Figure 6 portrays the variations of confinement loss spectra as a function of wavelength when the refractive index of the analyte is varied from 1.33 to

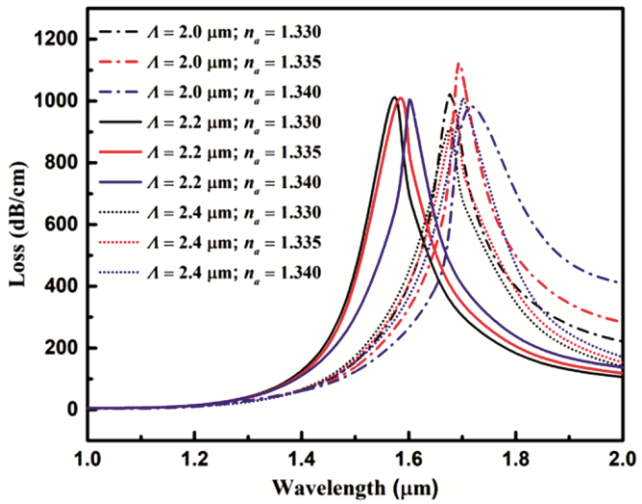


Fig. 5 — Loss spectra for the varying pitch for varying analyte refractive index from 1.33 to 1.34

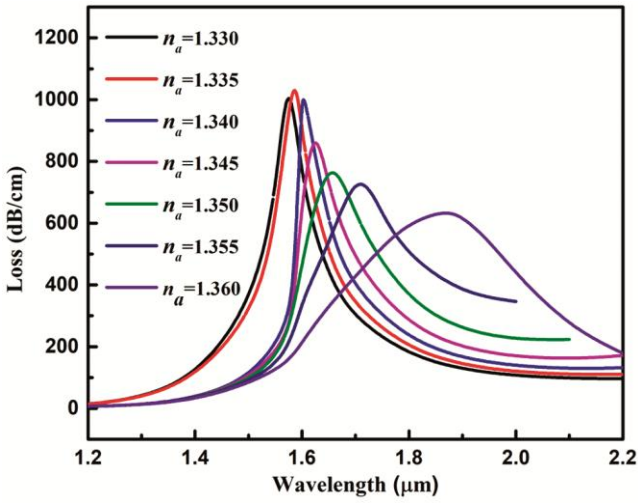


Fig. 6 — Variation of confinement loss as function of wavelength for analyte refractive index range from 1.33 to 1.36 in steps of 0.005

1.36 in steps of 0.005. From Fig. 6, we observe a set of seven resonant wavelengths at 1574, 1586, 1603, 1624, 1654, 1705 and 1864 nm with their corresponding refractive index of analytes being 1.33, 1.335, 1.34, 1.345, 1.35, 1.355 and 1.36. Further from Fig. 6, it is very clear that the peak of the confinement loss gets shifted towards longer wavelengths when the refractive index of the analyte is increased. In addition, it is found that the peak loss decreases with the increase in refractive index of the analyte. Here, the high/low loss indicates a more /less energy transfer from the fundamental mode to the surface plasmon mode. This is mainly because of the confinement of the fundamental mode field increasing with increase in refractive index of the analyte. A maximum wavelength shift of 159 nm occurs when the RI of analyte is varied from 1.355 to 1.36. Thus, the proposed SPR sensor exhibits a maximum sensitivity of 31,800 nm/RIU.

Next, we calculate the resolution of the proposed sensor. For a given instrumental peak-wavelength resolution of $\Delta\lambda_{min}$ = 0.1nm, the refractive index resolution of the corresponding sensor can be computed by using the following relation,

$$R = \frac{\Delta n_a \, \Delta\lambda_{min}}{\Delta\lambda_{peak}}(RIU), \quad \ldots (5)$$

Where, $\Delta n_a$ is the difference in refractive index of analyte and $\Delta\lambda_{peak}$ is the difference in peak resonant wavelength. Thus, we find that the proposed sensor showsa maximum resolutionof $3.14\times10^{-6}$RIU for a sensing range of 1.33 to 1.36.

The amplitude sensitivity of the proposed sensor for the varying analyte refractive index from 1.33 to 1.355 is shown in Fig. 7. The amplitude sensitivity is calculated using the formula[18],

$$S_A(\lambda) = -\frac{1}{\alpha(\lambda,n_a)}\frac{\partial\alpha(\lambda,n_a)}{\partial n_a}RIU^{-1} \quad \ldots (6)$$

Here, $\alpha(\lambda, n_a)$ is the initial confinement loss, $\partial\alpha(\lambda, n_a)$ is the difference between the adjacent confinement losses and $\partial n_a$ is the difference between the adjacent analyte refractive indices. Here, we find that the proposed sensor exhibits an amplitude sensitivity of 121 $RIU^{-1}$.

Apart from sensitivity, figure of merit (FOM), signal to noise ratio (SNR) and detection limit ($\delta n$) have been computed for the proposed sensor using the following expressions[35],

$$FOM = \frac{S(\lambda)}{FWHM} \quad \ldots (7)$$

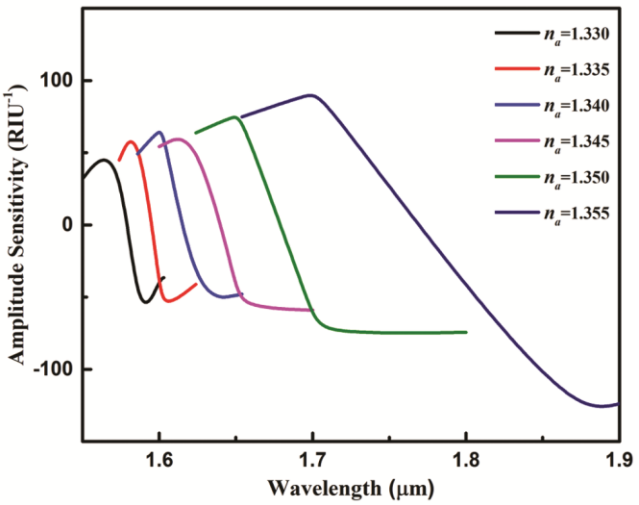


Fig. 7 — Amplitude sensitivity for the varying analyte refractive index

$$SNR = \frac{\Delta\lambda_{res}}{FWHM} \quad \ldots (8)$$

$$\delta_n = \frac{FWHM}{1.5(SNR)^{0.25}} \quad \ldots (9)$$

Here, FWHM is the full width half maximum of the loss curve and $\Delta\lambda_{res}$ is the difference in the adjacent peak resonant wavelength. The resonant wavelength, peak loss, FWHM, wavelength sensitivity, SNR, detection limit and figure of merit for the corresponding range of analyte RI for the proposed D shaped PCF SPR sensor are presented in Table 1.

The sensing comparison of the proposed sensor with that of the previously reported D-shaped PCF sensor is provided in Table 2. It can be observed from the table that the proposed sensor shows a better performance than the previously reported sensors.

## 5 Robustness of the proposed sensor

As discussed in Sections 3 and 4, the proposed sensor exhibits a maximum sensitivity only for the optimized structural parameters. In this section, we intend investigating the fabrication tolerance of (± 5%) the proposed sensor by varying the optimized parameters[42].

It is already reported that the fiber based plasmonic sensors are highly sensitive to the variations in the structural parameters. Therefore, it is of great interest to analyze influence of these structural parameters over the resonant loss spectra. In this section, we delineate the influence of mainly three structural parameters, namely, first ring air hole diameter, pitch and gold layer thickness over the resonant loss

Table 1 — Performance analysis of the proposed SPR PCF sensor for various analytes

| Analyte Refractive Index | Resonant Wavelength (nm) | Peak Loss (dB/cm) | Sensitivity (nm/RIU) | FWHM Loss Bandwidth (nm) | FOM | SNR | Detection Limit |
|---|---|---|---|---|---|---|---|
| 1.33 | 1574 | 1168.243 | 2400 | 11.8 | 203.3889 | 1.0169 | 7.833 |
| 1.335 | 1586 | 1182.792 | 3400 | 11.062 | 307.358 | 1.5367 | 6.6236 |
| 1.34 | 1603 | 1034.473 | 4200 | 4.923 | 853.138 | 4.2656 | 2.2837 |
| 1.345 | 1624 | 945.522 | 6000 | 9.639 | 622.471 | 3.1123 | 4.8380 |
| 1.35 | 1654 | 869.009 | 10200 | 10.509 | 970.596 | 4.8529 | 4.7203 |
| 1.355 | 1705 | 796.625 | 31800 | 34.688 | 916.743 | 4.5837 | 15.804 |
| 1.36 | 1864 | 641.466 | NA | 42.151 | NA | NA | NA |

Table 2 — Sensing comparison of the proposed sensor with the previously reported PCF sensors

| Fiber Characteristics and Ref. | Active metal | Wavelength (nm) | Analyte Range | Wavelength Sensitivity (nm/RIU) | Resolution Wavelength Inter. (RIU) | Amplitude Sensitivity ($RIU^{-1}$) |
|---|---|---|---|---|---|---|
| Square lattice PCF[19] | Gold | 700-1600 | 1.345-1.41 | 12,450 | N/A | N/A |
| Three core PCF[22] | Gold | 600-950 | 1.33-1.40 | 3435 | $2.91\times10^{-6}$ | 5059 |
| Birefringent six-core PCF sensor[25] | Gold | 1532 -2020 | 1.372, 1.432 | 8083 | $5.98\times10^{-6}$ | 226 |
| D-shaped PCF with V-groove analyte Channel[26] | Gold | 550-1900 | 1.33-1.43 | 31600 | $3.16\times10^{-6}$ | 550 |
| Analyte filled PCF sensor[36] | Gold | 1200-1800 | 1.40-1.42 | 7040 | N/A | N/A |
| Copper-Graphene-PCF Biosensor[37] | Copper-Graphene | 520-770 | 1.33-1.37 | 2000 | $5 \times 10^{-5}$ | N/A |
| Grapefruit Fiberwith Bimetallic Structure[38] | Silver and gold | 480-650 | 1.33-1.37 | 16,400 | $2.7\times10^{-5}$ | 216 |
| D-shaped photonic crystal fiber RI sensor[39] | Gold | 1200-3000 | 1.33-1.38 | 10,493 | $9.53\times10^{-6}$ | N/A |
| Gold grating-based PCF[40] | Gold | 550-1770 | 1.36-1.38 | 3,344 | $5.98\times10^{-6}$ | N/A |
| Dual-core D-shaped SPR sensor[41] | Titanium | 2100-3000 | 1.27-1.34 | 12,320.10 | $1.5 \times 10^{-2}$ | 230 |
| Proposed Sensor | Gold | 1200-2000 | 1.33-1.36 | 31800 | $3.14\times10^{-6}$ | 121 |

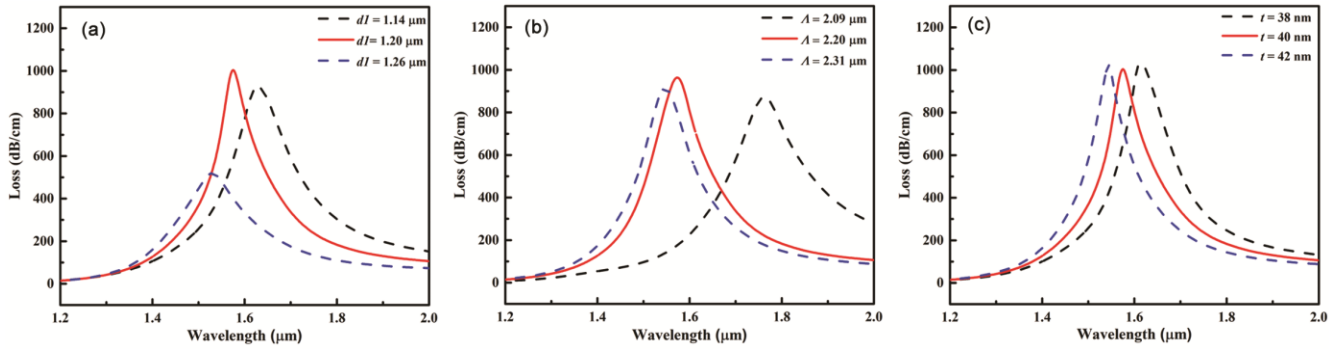


Fig. 8 — Analysis of fabrication tolerance of the proposed sensor by varying (a) first ring air hole diameter, (b) pitch (c) gold layer thickness

spectra. First, we study the variation of loss spectra for various values of air hole diameter. Figure 8(a) shows the effect of air hole diameter over the loss spectra. It is seen that there is a red shift in the peak wavelength when d1 is decreased and the peak loss decreases. On the other hand, when d1 is increased, loss spectrum undergoes blue shift and loss decreases drastically. Thus, the proposed sensor seems to be little sensitive for the variations in diameter of the first ring air hole. Next, we analyze the influence of pitch. Figure 8(b) shows the tolerance effect when the pitch is varied from the optimized value. From Fig. 7 (b), there is no appreciable change in peak loss when pitch is varied. Figure 8(c) portrays variations of loss spectra when gold layer thickness is varied. In this case also, there is no appreciable change in peak loss when the gold layer thickness is varied. Thus, these numerical results reveal that the proposed D-shaped PCF sensor is highly robust against the structural parameters.

## 6 Conclusion

In this paper, we have designed a compact and highly efficient plasmonic sensor using a commercially available D-shaped photonic crystal fiber. The proposed sensor exhibits a maximum

sensitivity of 31,800 nm/RIU with a resolution of $3.14\times10^{-6}$ RIU when the refractive index is varied from 1.355 to 1.36. First, we have investigated the physical mechanism of the proposed sensor by analyzing the loss spectra and the dispersion relations of fundamental mode and plasmonic mode. A rigorous numerical analysis has been carried out in order to optimize the various structural parameters, namely, first ring air hole diameter, pitch and gold layer thickness. Besides, by considering practical implementation of the proposed sensor, we have carried out the fabrication tolerance of ± 5% of the proposed sensor by varying the optimized structural parameters. The numerical results corroborate that the proposed sensor is highly robust against the variations in the structural parameters. We envisage that the proposed sensor could easily be realized with the commercially available D-shaped photonic crystal fiber. Further, we firmly believe that it would be highly useful in various fields of science, engineering and medicine.

## References


1 Liedberg B, Nylander C & Lunström I, *Sens Actuators*, 4 (1983) 299.
2 Villuendas F & Pelayo J, *Sens Actuators A Phys*, 23 (1990) 1142.
3 Piliarik M L, Parov´a´ & Homola J, *Biosens Bioelectron*, 24 (2009) 1399.
4 Homola J, *Frontiers in Planar Lightwave Circuit Technology*, Springer, (2006) 101.
5 Nivedha S, Ramesh Babu P & Senthilnathan K, *Current Science*,115 (2018) 56.
6 Homola J, *Anal Bioanal Chem*, 377 (2003) 528.
7 Wood R W, *Proc Phys Soc* London, 18 (1902) 269.
8 Otto A, *Z Phys*, 216 (1968) 398.
9 Kretschmann E & Raether H, *Z Naturforsch A*, 23 (1968) 2135.
10 Jorgenson R & Yee S, *Sens Actuators B Chem*,12 (1993) 213.
11 Homola J & Slavik R, *Electron Lett*, 32 (1996) 480.
12 Russell P, *Science*, 299 (2003) 358.
13 Sharma M, Borogohain N & Konar S, *IEEE J Lightwave Tech*, 31 (2013) 3339.
14 Chen H L, Li S G, Fan Z K, An G W, Li J S & Han Y, *IEEE Photon J*, 6 (2014) 6803006.
15 Villatoro J, Finazzi V, Minkovich V P, Pruneri V& Badenes G, *Appl Phys Lett*, 91 (2007) 091109.
16 Pinto A M R & Lopez A M, *J Sensors*, (2012) 1.
17 Tian M, Lu P, Chen L, Lv C& Li D, *Opt Commun*, (2012) 285.
18 Rifat A A, Ahmed R, Mahdiraji G A & Adikan F M, *IEEE Sens J*, 17 (2017) 2776.
19 Wang G, Li S, An G, Wang X, Zhao Y, Zhang W & Chen H, *Opt Quant Electron*, 48 (2016) 46.
20 Gangwar R K & Singh V K, *Plasmonics*, 12 (2017) 1367.
21 Hasan M R, Akter S, Rifat A A, Rana S, Ahmed K, Ahmed R, Subbaraman H & Abbott D, *IEEE Sens J*, 18 (2017) 133.
22 Tong K, Wang F, Wang M, Dang P & Wang Y, *Opt Fiber Technol*, 46 (2018) 306.
23 Zhou X, Cheng T, Li S, Suzuki T & Ohishi Y, *OSA Continuum*, 1 (2018) 1332.
24 Sakib M N, Hossain M B, Al-tabatabaie K F, Mehedi I M, Hasan M T, Hossain M A & Amiri IS, *Results Phys*, 15 (2019) 102788.
*25* Liao J, Xie Y, Huang T, Ding Z, Zeng M, Wu S & Hu X, *J Mod Opt*, (2020) 1.
26 Melwin G & Senthilnathan K, *Optik*, 213 (2020) 164779.
27 Adams M J, An introduction to optical waveguides (Wiley, New York) 1981.
28 Singh S & Gupta B D, *Meas Sci Technol*, 21 (2010) 1152021.
29 `Yang Z, Xia L, Li C, Chen X & Liu D, *Opt Commun*, 430 (2019) 195.
30 Zhang N, Li K, Cui Y, Wu Z, Shum P P, Auguste J L, Dinh X Q, Humbert G & Wei L, *Lab Chip*, 18 (2018) 655.
31 Huang T, *Plasmonics*, 12 (2017) 583.
32 Boehm J, François A, Ebendorff-Heidepriem H & Monro T M, *Plasmonics*, 6 (2011) 133.
33 Peng L, Shi F, Zhou G, Ge S, Hou Z & Xia C, *IEEE Photon J*, 7 (2015) 1.
34 Rifat A A, Mahdiraji G A, Chow D M, Shee Y G, Ahmed R & Adikan F R, *Sensors*, 15 (2015) 11499.
35 Shaban M, Ahmed A M, Abdel-Rahman E & Hamdy H, *Scientific Rep*, 7 (2017) 1.
36 Fan Z, Li S, Liu Q, An G, Chen H, Li J, Chao D, Li H, Zi J & Tian W, *IEEE Photon J*, 7 (2015) 1.
37 Rifat A A, Mahdiraji G A, Ahmed R, Chow D M, Sua Y M, Shee YG & Adikan F M, *IEEE Photon J*, 8 (2015) 1.
38 Yang X, Lu Y, Wang M & Yao J, *IEEE Photon Technol Lett*, 28 (2016) 649.
39 An G, Hao X, Li S, Yan X & Zhang X, *Appl opt*, 56 (2017) 6988.
40 Lu J, Li Y, Han Y, Liu Y & Gao J, *Appl Opt*, 57 (2018) 5268.
41 Jabin M A, Ahmed K, Rana M J, Paul B K, Luo Y & Vigneswaran D, *Plasmonics*, 14 (2019) 1601.
42 Chang M, Li B, Chen N, Lu X, Zhang X & Xu J, *IEEE Photon J*, 11 (2019) 7202312.